annalen der physik
www.ann-phys.org

Out-of-Time-Order Correlators and Quantum Phase Transitions in the Rabi and Dicke Models

Zheng-Hang Sun, Jia-Qi Cai, Qi-Cheng Tang, Yong Hu, and Heng Fan**

The out-of-time-order correlators (OTOCs) is used to study the quantum phase transitions (QPTs) between the normal phase and the superradiant phase in the Rabi and few-body Dicke models with large frequency ratio of the atomic level splitting to the single-mode electromagnetic radiation field frequency. The focus is on the OTOC thermally averaged with infinite temperature, which is an experimentally feasible quantity. It is shown that the critical points can be identified by long-time averaging of the OTOC via observing its local minimum behavior. More importantly, the scaling laws of the OTOC for QPTs are revealed by studying the experimentally accessible conditions with finite frequency ratio and finite number of atoms in the studied models. The critical exponents extracted from the scaling laws of OTOC indicate that the QPTs in the Rabi and Dicke models belong to the same universality class.

1. Introduction

The equilibrium phases of matter and quantum phase transitions (QPTs) are conventionally understood by broken symmetries[1] and their topologies.[2] Regarding the rapid development in quantum technologies, the nonequilibrium properties of many-body quantum systems can be studied by large-scale quantum simulators.[3,4] The dynamics of several quantities, such as the quantum correlations[5] and order parameters,[4,6,7] play an important role in characterizing the quantum criticality and may serve as a bridge from the equilibrium phases to the nonequilibrium behaviors of systems.

Recently, the out-of-time-order correlators (OTOCs),[8–10] which quantify the quantum chaos,[11–14] information scrambling,[15–22] and many-body localization,[23–28] have also been exploited in detecting the QPTs. The Lyapunov exponent obtained from the dynamical behavior of OTOC with thermal average has a maximum near the quantum critical region.[29,30] In addition, it has been shown that the OTOCs with respect to the ground states and quenched states can diagnose the QPTs and dynamical phase transition, respectively.[31] Meanwhile, great progresses have been achieved for experimental observation of the OTOCs by employing inverse-time evolution.[32,33]

The Dicke and Rabi models, which are fundamental models in quantum optics, reveal a universality class of QPT from largely unexcited normal phase to superradiant phase in the case of the thermodynamic limit[34–38] and infinite atomic level splitting in the unit of the single-mode light field frequency,[39–43] respectively. The critical exponents obtained from the scaling laws of corresponding observables for the ground states in the Rabi and Dicke models are found to be the same.[39,40,44,45] This fact implies that there exists a wide class of observables whose scaling behaviors associated with the finite-size and finite-frequency effect can be observed near the critical points of these models.

Although the OTOCs are closely related to the QPTs in condensed-matter systems, it is not clear whether the OTOCs can detect the QPT between the normal phase and the superradiant phase in cavity–atom interaction systems. The Rabi and Dicke models can be experimentally realized in the ultracold atoms,[46–49] trapped ions,[50,51] the superconducting circuits,[52,53] as well as the photonic system,[54] where the time evolutions of the observables are naturally accessible. The QPTs between normal phase and superradiant phase in the Dicke and Rabi models are observed via adiabatic evolution of the order parameter.[46,47,51] Additionally, we recognize that the quench dynamics[50] or the initialization into thermal equilibrium states[33] are also accessible in some experimental platforms. On the other hand, the universality and scaling exponents play important roles for our comprehension of QPTs.[1] Consequently, it is important to develop the OTOC method as a new dynamical way of characterizing the QPTs besides the adiabatic protocol, and clarify whether the scaling laws can be obtained from the behaviors of OTOCs close to the critical points.

Z.-H. Sun, Prof. H. Fan
Institute of Physics
Chinese Academy of Sciences
Beijing 100190, China
E-mail: hfan@iphy.ac.cn
Z.-H. Sun, Prof. H. Fan
School of Physical Sciences
University of Chinese Academy of Sciences
Beijing 100190, China
J.-Q. Cai, Prof. Y. Hu
School of Physics
Huazhong University of Science and Technology
Wuhan 430074, China
E-mail: huyong@hust.edu.cn
Q.-C. Tang
School of Science
Westlake University
Hangzhou 310024, China
Prof. H. Fan
CAS Centre for Excellence in Topological Quantum Computation
Beijing 100190, China

DOI: 10.1002/andp.201900270

 © 2020 WILEY-VCH Verlag GmbH & Co. KGaA, Weinheim

In this work, we show that: i) the OTOCs can detect the QPT between normal phase and superradiant phase in the Rabi model and the Dicke model with small number of atoms. Specifically, taking the experimental accessibility into consideration, we mainly study the OTOC with infinite temperature thermal average. We find that the local minimum point of time-averaged infinite-temperature OTOC coincides with the critical point. Therefore, it has the potential to be a dynamical probe of QPTs. ii) Our numerical results also reveal several scaling laws of the studied OTOC, paving the way for extracting significant information of the QPTs in few-body systems, such as the universality class and the location of critical point in the thermodynamic limit or large frequency ratio limit. In short, our results provide an experimentally feasible approach to detect equilibrium quantum critical points and the universality of QPTs.

2. Results

2.1. Definition

The OTOCs are defined as[8–10]

$$\mathcal{F}(t) = \langle \hat{W}^{\dagger}(t)\hat{V}^{\dagger}(0)\hat{W}(t)\hat{V}(0)\rangle \tag{1}$$

with two commuting Hermitian operators at equal time, that is, $[\hat{W}(0), \hat{V}(0)] = 0$, and $\hat{W}(t) = e^{i\hat{H}t}\hat{W}(0)e^{-i\hat{H}t}$. The average $\langle\mathcal{O}\rangle$ above can be chosen as the thermal average $\langle\mathcal{O}\rangle_{\beta} = \mathrm{Tr}(e^{-\beta H}\mathcal{O})/\mathrm{Tr}(e^{-\beta H})$ with the inverse temperature $\beta = 1/T$, or the state average $\langle\mathcal{O}\rangle_{|\psi\rangle} = \langle\psi|\mathcal{O}|\psi\rangle$ with a given pure state $|\psi\rangle$.

2.2. OTOCs in the Rabi Model

We first study the OTOC in the Rabi model with Hamiltonian as

$$\mathcal{H}_{\mathrm{Rabi}} = \omega_0 a^{\dagger}a + \frac{\Omega}{2}\sigma_z + g(a^{\dagger} + a)\sigma_x \tag{2}$$

where ω_0 denotes the frequency of the single-mode light field, and the level splitting of a single two-level atom is Ω, g denotes the coupling strength between the light field and the atom. The critical coupling strength of the ground state QPT is $g_c = \sqrt{\omega_0\Omega}/2$, when the QPT happens in the limit of frequency ratio $\eta = \Omega/\omega_0 \to \infty$.[39,40] Here we emphasize that when we discuss the QPTs in the Rabi model, although strictly speaking, the limit $\eta \to \infty$ is not the thermodynamic limit, it plays a similar rule of thermodynamic limit. Hence, we adopt relatively large values of $\eta = 2^{11}, 2^{12}, \ldots, 2^{20}$ to investigate the characterization of QPT in the Rabi model via infinite-temperature OTOC and related scaling laws. The quantum Rabi model explicitly breaks the parity symmetry $\Pi = \exp\{i\pi(a^{\dagger}a + \frac{1+\sigma_z}{2})\}$. Thus, the QPT of this model can be understood by symmetry broken theory.[1] The system breaks Π when $g \geq g_c$ and recovers its symmetry when $g \leq g_c$.[39]

We choose the operators in Equation (1) $\hat{W} = \hat{V} = a^{\dagger}a$ as the order parameter of this model to define the OTOCs. Here, we realize that the OTOCs may provide nontrivial information of quench dynamics because the eigenstates of $\mathcal{H}_{\mathrm{Rabi}}$ are not necessarily the eigenstates of $a^{\dagger}a$. The exact analytical solution of quenched dynamics instead of adiabatic evolution for the Rabi model is still a complex open problem, and we would numerically study the OTOCs Equation (1) in the considered models based on exact diagonalization method (the functions "propagator" and "Q.groundstate()" in QuTiP are used to get $U(t) = e^{-i\hat{H}t}$ and the ground state $|\psi\rangle$ of $\hat{H}$, and the thermal average $\langle\mathcal{O}\rangle_{\beta}$ can also be calculated when we obtain all the eigenenergies and eigenstates of $\hat{H}$ using the functions "Q.eigenenergies()" and "Q.eigenstates()" in QuTiP[55]). The python codes used to generate our results are presented in the Supporting Information.[56] We believe that the following numerical results are valuable for the reference of further analytical works.

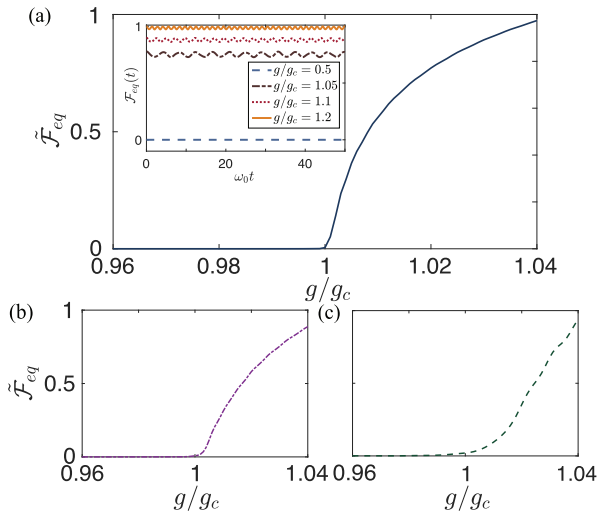

Figure 1. a) The dependence of time-averaged equilibrium OTOC $\tilde{\mathcal{F}}_{\mathrm{eq}}$ and g/g_c. The time window of the average is $t_f \approx 500\omega_0$ and the frequency ratio in the Rabi model is $\eta = 2^{20}$. Here, the number of cavity photons is $n = 80$. Inset: The time evolution of equilibrium OTOC $\mathcal{F}_{\mathrm{eq}}(t)$. b,c) Similar to (a) but for the Rabi model with $n = 40$ and $n = 20$, respectively. The values of $\tilde{\mathcal{F}}_{\mathrm{eq}}$ are rescaled by the $\tilde{\mathcal{F}}_{\mathrm{eq}}$ at $g/g_c = 1.2$.

In **Figure 1**a, the time-averaged equilibrium OTOC $\tilde{\mathcal{F}}_{\mathrm{eq}} = \frac{1}{t_f}\int_0^{t_f} dt\mathcal{F}_{\mathrm{eq}}(t)$ as a function of g/g_c is presented, which indicates that $\tilde{\mathcal{F}}_{\mathrm{eq}}$ can detect the QPT in Rabi model. In fact, it is obvious that the value of $\mathcal{F}_{\mathrm{eq}}(t)$ at any time t can highlight the critical point. We then study the dependence of $\mathcal{F}_{\mathrm{eq}}(t)$ and the cutoff on the number of cavity photons n (also as the dimension of the operator $a^{\dagger}a$). The results for $n = 40$ and $n = 20$ are shown in Figure 1b,c, respectively, while in Figure 1a, $n = 80$ as relatively large value. One can see that the signature of QPT diagnosed by the equilibrium OTOC becomes less distinguishable for small n. Thus, in the following study, we will choose a large value of n and benchmark the finite-n effect (see Figure **4** for the other type of OTOC.)

Nevertheless, efficiently acquiring the ground state of a system, as a necessity for evaluating the equilibrium OTOC,[32] is still a challenge in several experimental platforms.[57,58] Fortunately, the OTOC thermally averaged with $\beta = 0\mathcal{F}_{\beta=0}(t) = \mathrm{Tr}[\hat{W}^{\dagger}(t)\hat{V}^{\dagger}(0)\hat{W}(t)\hat{V}(0)]$ (the partition function $Z = \mathrm{Tr}(e^{-\beta H})$ with $\beta = 0$ is independent of the coupling strength

© 2020 WILEY-VCH Verlag GmbH & Co. KGaA, Weinheim

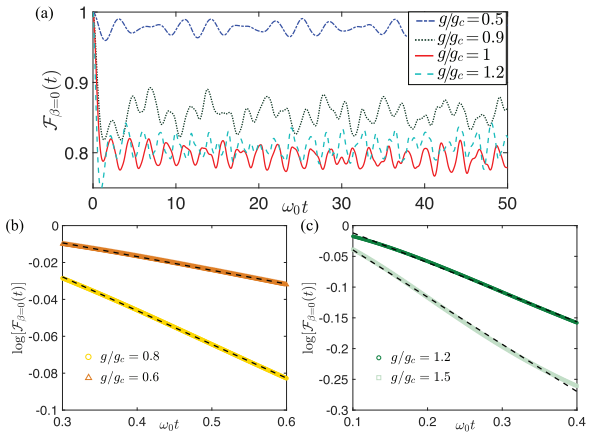

Figure 2. a) The time evolution of infinite-temperature OTOC $\mathcal{F}_{\beta=0}(t)$ (normalized). b) The dynamical behaviors of $\log(\mathcal{F}_{\beta=0}(t))$ in Rabi model with $g/g_c = 0.8$, 0.6 and time interval $t \in [0.3\omega_0, 0.6\omega_0]$. The dashed lines are linear fittings. c) is similar to b) but with $g/g_c = 1.2$, 1.5 and time interval $t \in [1.2\omega_0, 1.5\omega_0]$.

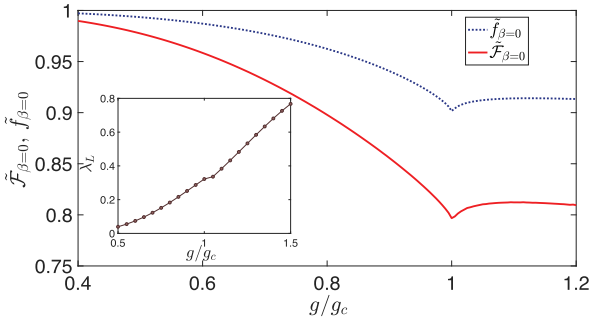

Figure 3. The dependence of time-averaged infinite-temperature OTOC $\tilde{\mathcal{F}}_{\beta=0}$ (normalized) as well as two-point correlator $\tilde{f}_{\beta=0}(t)$ (normalized), and g/g_c. The time window of the average is $t_f \approx 500\omega_0$ and the frequency ratio in the Rabi model is $\eta = 2^{20}$. The inset shows the Lyapunov-like exponent extracted from the time evolution of $\mathcal{F}_{\beta=0}(t)$ as a function of g/g_c.

g and thus is omitted) can be measured in the NMR quantum simulator[33] by applying the distinguishability protocol.[16] Here, the quantity $\mathcal{F}_{\beta=0}(t)$ is named after infinite-temperature OTOC.

In order to study the relation between infinite-temperature OTOC and the QPT in Rabi model, we numerically calculate the time evolution of infinite-temperature OTOC $\mathcal{F}_{\beta=0}(t)$ with the frequency ratio $\eta = 2^{20}$, which are depicted in **Figure 2**a. As shown in Figure 2b,c, in the beginning of the time evolution of the OTOC $\mathcal{F}_{\beta=0}(t)$, it decays exponentially, that is, $\mathcal{F}_{\beta=0}(t) \approx \exp(-\lambda_L t)$. Consequently, $\log(\mathcal{F}_{\beta=0}(t)) \propto -\lambda_L t$ and the slope is Lyapunov-like exponents λ_L. We chose the appropriate time interval to ensure that $\log(\mathcal{F}_{\beta=0}(t)) \propto -\lambda_L t$ is satisfied. For instance, we fit the data of $\log(\mathcal{F}_{\beta=0}(t))$ with $t \in [0.3\omega_0, 0.6\omega_0]$ for $0.5 \leq g/g_c \leq 1$ and with $t \in [0.1\omega_0, 0.4\omega_0]$ for $g/g_c \geq 1.1$. The relation between λ_L and g/g_c is shown in the inset of **Figure 3**, which indicates that the λ_L with $\beta = 0$ cannot reveal the information of QPT.

Next, the time average of infinite-temperature OTOC $\tilde{\mathcal{F}}_{\beta=0} = \frac{1}{t_f}\int_0^{t_f} dt\mathcal{F}_{\beta=0}(t)$ is discussed. In Figure 2a, because of the integrability of Rabi model,[59] drastic oscillation can be observed in the

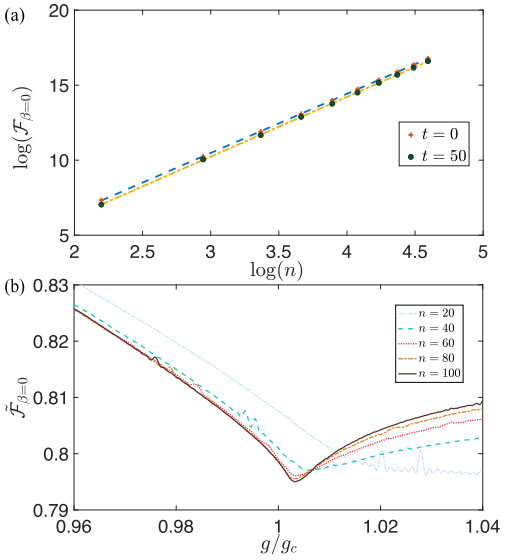

Figure 4. a) The $\log(\mathcal{F}_{\beta=0})$ as a function of $\log(n)$ for time $t = 0$ and $t = 50$, where $\mathcal{F}_{\beta=0}$ is the bare value of OTOC and n is the maximum photon cutoff. The fitting curves for $t = 0$ and $t = 50$ are $\log(\mathcal{F}_{\beta=0}) \propto 3.98\log(n)$ and $\log(\mathcal{F}_{\beta=0}) \propto 3.95\log(n)$, respectively, which indicates that $\mathcal{F}_{\beta=0}(t) \approx n^4$. b) The time-averaged infinite-temperature OTOC $\tilde{\mathcal{F}}_{\beta=0}$ as a function of g/g_c in the Rabi model with $\eta = 2^{20}$ and different dimensions of operator $a^\dagger a$ $n = 20, 40, 60, 80, 100$.

dynamics of $\mathcal{F}_{\beta=0}(t)$. Therefore, the long-time average is required for extracting the signature of QPT. We present the results of $\tilde{\mathcal{F}}_{\beta=0}$ with the time window $t_f \approx 500\omega_0$ as a function of g/g_c in Figure 3. Here, the value of $\tilde{\mathcal{F}}_{\beta=0}$ is normalized by $\tilde{\mathcal{F}}_{\beta=0}/\mathcal{F}_{\beta=0}(t = 0) = \tilde{\mathcal{F}}_{\beta=0}/\mathrm{Tr}[W^\dagger(0)V^\dagger(0)W(0)V(0)]$. Remarkably, there is a local extreme point of $\tilde{\mathcal{F}}_{\beta=0}$ close to the critical point $g/g_c = 1$, which might be regarded as a signature of QPT and should be further ensured by studying the scaling behaviors of the $\tilde{\mathcal{F}}_{\beta=0}$. The comparison between λ_L extracted from the short-time behaviors of $\mathcal{F}_{\beta=0}(t)$ and $\tilde{\mathcal{F}}_{\beta=0}$ indicates the necessity of longer-time average of OTOC for the detection of QPT.

As a side remark, a recent work, where the two-point correlators (TPCs) in the Sachdev–Ye–Kitaev model and disordered XXZ model are studied, has revealed that the TPCs can characterize quantum chaos and can be regarded as an alternative to OTOCs.[60] In Figure 3, we show that the infinite-temperature TPCs defined as $f_{\beta=0} = \mathrm{Tr}[W(t)V(0)]$ with $\hat{W} = \hat{V} = a^\dagger a$ can also detect the QPT in the Rabi model via its time average $\tilde{f}_{\beta=0}(t) = \frac{1}{t_f}\int_0^{t_f} dt f_{\beta=0}(t)$ with $t_f \approx 500\omega_0$. However, the infinite-temperature OTOC is more sensitive to g/g_c and the critical behavior is more distinct because the value of $\tilde{\mathcal{F}}_{\beta=0}$ at the critical point $g/g_c = 1$ is smaller than that of $\tilde{f}_{\beta=0}(t)$.

In order to intuitively understand the normalization of $\tilde{\mathcal{F}}_{\beta=0}$, here we present how the value of infinite-temperature OTOC without normalization scales with the cavity photon number n. As shown in **Figure** 4a, with the increase of n, both the $\mathcal{F}_{\beta=0}(t)$ at $t = 0$ and $t = 50$ increase with the form of $\mathcal{F}_{\beta=0}(t) \approx n^4$. In the limit of $n \to \infty$, the values of $\mathcal{F}_{\beta=0}(t)$ tend to infinity. Nevertheless, the ratio $\mathcal{F}_{\beta=0}(t = 50)/\mathcal{F}_{\beta=0}(t = 0)$ remains a finite value and

© 2020 WILEY-VCH Verlag GmbH & Co. KGaA, Weinheim

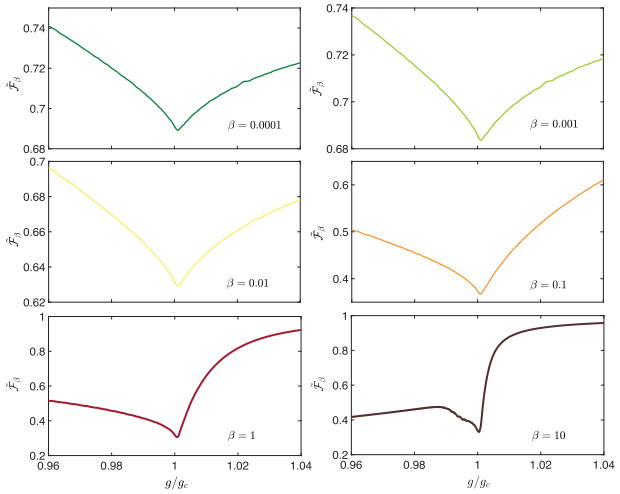

Figure 5. The time-averaged thermal OTOC $\tilde{\mathcal{F}}_\beta$ (rescaled by $\tilde{\mathcal{F}}_\beta/\tilde{\mathcal{F}}_\beta(0)$) in the Rabi model as a function of g/g_c with $\eta = 2^{20}$ and different finite values of β.

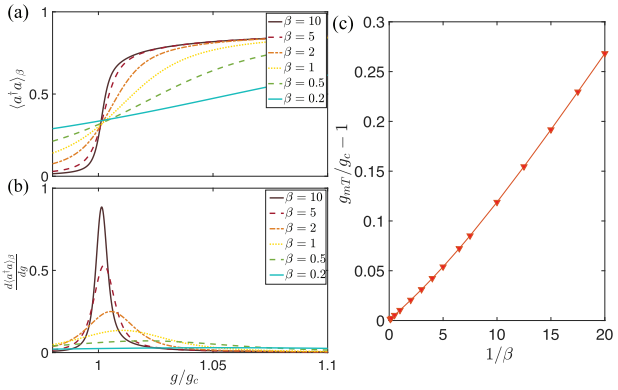

Figure 6. a) The thermal average of order parameter $\langle a^\dagger a\rangle_\beta$ with different inverse-temperature $\beta = 1/T$ in the Rabi model as a function of g/g_c with $\eta = 2^{20}$. b) Similar to (a) but for the susceptibility of $\langle a^\dagger a\rangle_\beta$ with respect to g, that is, $\frac{d\langle a^\dagger a\rangle_\beta}{dg}$. c) The location of maximum point of $\langle a^\dagger a\rangle_\beta$ as a function of temperature T.

smaller than 1 because $\mathcal{F}_{\beta=0}(t) < \mathcal{F}_{\beta=0}(t=0)$ for any $t > 0$. Furthermore, we need to increase n to suppress the influence of the n effect. As depicted in Figure 4b, the $\tilde{\mathcal{F}}_{\beta=0}$ is trivial for $n = 20$. With the increase of n, the location of $\tilde{\mathcal{F}}_{\beta=0}$ minimum point tends to $g/g_c = 1$. The locations of $\tilde{\mathcal{F}}_{\beta=0}$ minimum point for $n = 60, 80$, and 100 are basically indistinguishable. Therefore, the finite-n effect on the behaviors of $\tilde{\mathcal{F}}_{\beta=0}$ can be neglected with $n \approx 80$.

It is well known that the thermal fluctuations can influence the QPT that occurs at zero temperature in principle.[1] For instance, the signatures of critical points dramatically change with the variation of β in several systems such as the Dicke model or Ising model.[37,61–64] However, as shown in **Figure 5**, it is remarkable that the local minimum points around $g/g_c = 1$ of the time-averaged thermal OTOC $\tilde{\mathcal{F}}_\beta$ remains the same, and the capability of $\tilde{\mathcal{F}}_\beta$ in detecting the QPT is independent of β. Meanwhile, the shape of the $\tilde{\mathcal{F}}_\beta$ as a function of g/g_c tends to the equilibrium OTOC depicted in Figure 1 with the increase of β. To compare the results of $\tilde{\mathcal{F}}_\beta$, we also calculate the thermal-averaged order parameter $\langle a^\dagger a\rangle_\beta$ and the results are shown in **Figure 6**. It can be obviously seen that the locations of $d\langle a^\dagger a\rangle_\beta/dg$ maximum point departure from the critical point g_c at $T = 0$. Thus, the signature of the QPT highlighted by the OTOC $\tilde{\mathcal{F}}_\beta$ is more robust against β than the order parameter. Actually, besides the thermal average in the definition of the OTOCs, more importantly, $\mathcal{F}_\beta(t)$ probes the operator spread $\hat{W}(t)$ overlapping with the other operator $\hat{V}$, as a nonequilibrium property of the system, and could encode more information than the time-independent quantity $\langle a^\dagger a\rangle_\beta$.

Although the Rabi model can be realized in many experimental platforms,[50–54] the limit $\eta \to \infty$ is unattainable in quantum simulation experiments. This motivates us to study the finite-η behaviors of $\tilde{\mathcal{F}}_{\beta=0}$ near the critical points. In **Figure 7**a, we observe that the location of $\tilde{\mathcal{F}}_{\beta=0}$ minimum point g_m/g_c is dependent on η and tends to $g_m/g_c = 1$ with the increase of η. As shown in Figure 7b, we obtain the scaling law

$$\log\left(\frac{g_m - g_c}{g_c}\right) \approx -k\log(\eta) \tag{3}$$

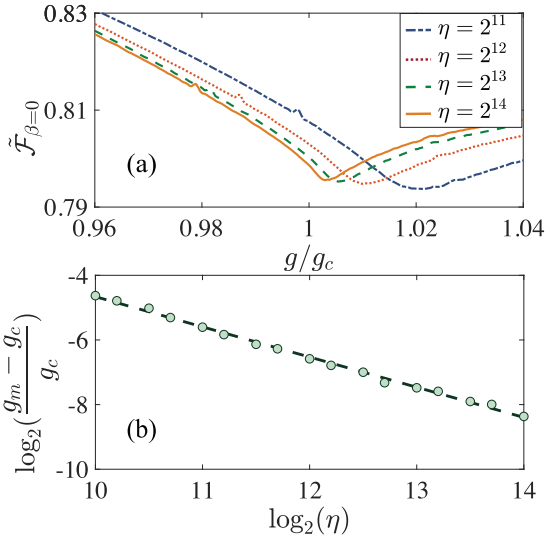

Figure 7. a) The time-averaged infinite-temperature OTOC $\tilde{\mathcal{F}}_{\beta=0}$ (rescaled by $\tilde{\mathcal{F}}_{\beta=0}/\mathcal{F}_{\beta=0}(0)$) as a function of g/g_c with several values of η in the Rabi model. b) The dependence of $\log_2(\frac{g_m - g_c}{g_c})$ and $\log_2(\eta)$ where g_m/g_c denotes the location of $\tilde{\mathcal{F}}_{\beta=0}$ minimum point. The green dashed line is the linear fitting $\log_2(\frac{g_m - g_c}{g_c}) \approx -0.952\log_2(\eta)$.

where the positive number k is the critical exponent of $\tilde{\mathcal{F}}_{\beta=0}$. The scaling law is of great importance. First, we can obtain the location of the critical point in the limit $\eta \to \infty$ from the data of $\tilde{\mathcal{F}}_{\beta=0}$ with finite η. Second, we can decode the information of universality class from the value of k. Because of the scaling law Equation (3), the emergence of a dip in $\tilde{\mathcal{F}}_{\beta=0}$ shown in Figure 2b is a signature of QPT.

2.3. OTOCs in the Dicke Model

The Rabi model can be generalized to the Dicke model by replacing single two-level atom with many two-level atoms. The

© 2020 WILEY-VCH Verlag GmbH & Co. KGaA, Weinheim

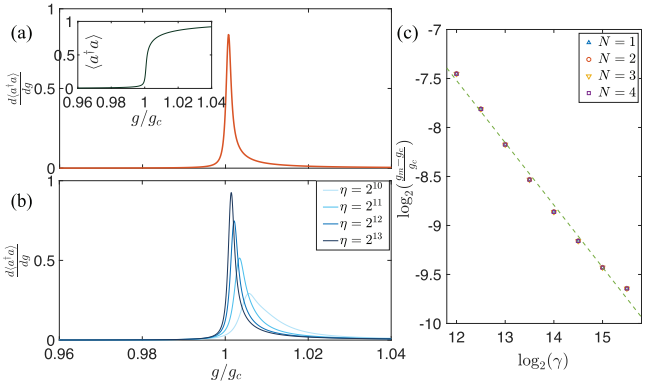

Figure 8. a) The value of $\frac{d\langle a^\dagger a\rangle}{dg}$ as a function of g/g_c. The inset shows the value of $\langle a^\dagger a\rangle$ (rescaled by the dimension of operator $a^\dagger a$ n) as a function of g/g_c. b) The value of $\frac{d\langle a^\dagger a\rangle}{dg}$ as a function of g/g_c for the Dicke model with $N = 4$ and $\Omega/\omega_0 = 2^{10}, 2^{11}, 2^{12}, 2^{13}$. c) The dependence of $\frac{g_m - g_c}{g_c}$, where g_m is the location of maximum point of $\frac{d\langle a^\dagger a\rangle}{dg}$, and $\gamma = \Omega N/\omega_0$ with $N = 1, 2, 4, 8$. The dashed line is linear fitting $\log_2[(g_m - g_c)/g_c] \approx -0.649 \log_2(\gamma)$.

Hamiltonian of the Dicke model is

$$\mathcal{H}^N_{\text{Dicke}} = \omega_0 a^\dagger a + \Omega J_z + \frac{g}{\sqrt{2j}}(a^\dagger + a)(J_+ + J_-) \tag{4}$$

where $N = 2j$ is the number of atoms. Due to the permutation symmetry, $J_{z,\pm} = \sum_{i=1}^{2j} \frac{1}{2}\sigma^i_{z,\pm}$ can be defined as the collective spin operators with length j.[65]

State-of-the-art technology allows us to manipulate and obtain the dynamical result from the Dicke model with relatively small N.[66] Thus, it is worthy of studying further if there exists a second-order QPT in the Dicke model with extremely large $\eta = \Omega/\omega_0$ in the case of a small number of atoms. In the inset of **Figure 8**a, we show that $\langle a^\dagger a\rangle = \langle\psi|a^\dagger a|\psi\rangle$ where the ground state $|\psi\rangle$ is zero in the normal phase and becomes a finite value in the superradiant phase, which is similar to $\langle a^\dagger a\rangle$ in the Rabi model.[39] Hence, a second-order QPT still exists in the few-body Dicke model in the limit $\eta \to \infty$ and $a^\dagger a$ is also a bona fide order parameter. As depicted in Figure 8a, there is a nonanalytical behavior for $d\langle a^\dagger a\rangle/dg$ diverges at the critical point $g/g_c = 1$. In ref. [34], it has been revealed that the behaviors of order parameter susceptibility for the QPT of the Dicke model tend to diverge with the increase of η or N, which is consistent with the results presented in Figure 8b. According to the dependence of g_m, as the location of the maximum point of $d\langle a^\dagger a\rangle/dg$, and η, we can obtain a quantitative relation $\log(\frac{g_m - g_c}{g_c}) \propto \log(\eta)$ whose formulation is the same as Equation (3). Furthermore, we demonstrate the relation for different N. As shown in Figure 8c, with the fixed $\gamma = \eta N = \Omega N/\omega_0$, g_c is independent of N, indicating that γ plays a more fundamental role in the studied QPTs and the generalized relation is $\log(\frac{g_m - g_c}{g_c}) \propto \log(\gamma)$. In fact, similar to the results shown in Figure 8c, the scaling functions studied in ref. [40] can also be generalized to $N > 1$.

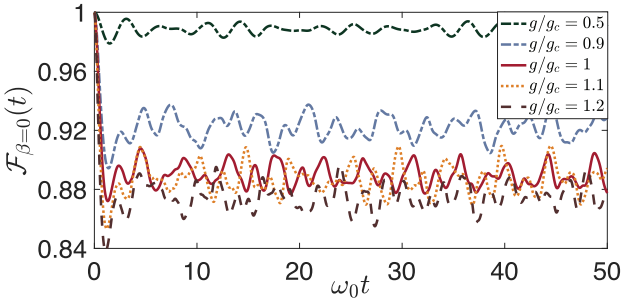

Figure 9. Time evolution for the infinite-temperature OTOC $\mathcal{F}_{\beta=0}(t)$ in the Dicke model with $\eta = 2^{20}$, $N = 4$, and $g/g_c = 0.5, 0.9, 1, 1.1$, and 1.2.

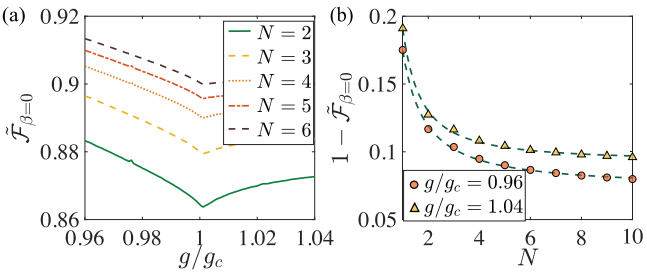

Figure 10. a) $\tilde{\mathcal{F}}_{\beta=0}$ (rescaled by $\tilde{\mathcal{F}}_{\beta=0}/\mathcal{F}_{\beta=0}(0)$) as a function of g/g_c in the Dicke model with different number of atoms N and $\eta = 2^{20}$. b) The value of $1 - \tilde{\mathcal{F}}_{\beta=0}$ as a function of N. The dashed lines are fitting curves with the formulation of Equation (5).

It is noted that various quantum optics experiments pay attention to the measurement of both adiabatic[46,47,51] and quench dynamics[67] of order parameter, trying to observe similar signatures shown in the inset of Figure 8a. However, for the purpose of experimentally studying the scaling law Equation (3), the cusp-like character of $\tilde{\mathcal{F}}_\beta$ in Figure 7a may be more convenient than the order parameter $\langle a^\dagger a\rangle$ because $\tilde{\mathcal{F}}_\beta$ can directly pinpoint the critical point of the QPT, while we should make a derivative of $\langle a^\dagger a\rangle$, as a requirement for higher accuracy of experimental data, to obtain the similar cusp-like character, see Figure 7b.

We then explore the linkage between the QPTs in the Dicke model and the infinite-temperature OTOC, as well as the related scaling laws. After calculating the dynamics of infinite-temperature OTOC shown in **Figure 9**, we can obtain the time-averaged infinite-temperature OTOC $\tilde{\mathcal{F}}_{\beta=0}$ as a function of g/g_c in the Dicke model with different N and $\eta = 2^{20}$. The results are depicted in **Figure 10**a. Similar to the behaviors of $\tilde{\mathcal{F}}_{\beta=0}$ in the Rabi model, we can also observe the local minimum point of $\tilde{\mathcal{F}}_{\beta=0}$ near $g/g_c = 1$ in the Dicke model. Consequently, the infinite-temperature OTOC is capable of identifying the critical point of QPT in the Dicke model with large η.

Moreover, the finite-N effect on the value of $\tilde{\mathcal{F}}_{\beta=0}$ is also studied. As shown in Figure 10b, with the increase of N, the value of $1 - \tilde{\mathcal{F}}_{\beta=0}$ at critical point decays as a power law

$$1 - \tilde{\mathcal{F}}_{\beta=0} = aN^{-b} + c \tag{5}$$

The coefficients a, b as functions of g/g_c are presented in **Figure 11**a,b respectively, which indicate that the coefficients

© 2020 WILEY-VCH Verlag GmbH & Co. KGaA, Weinheim

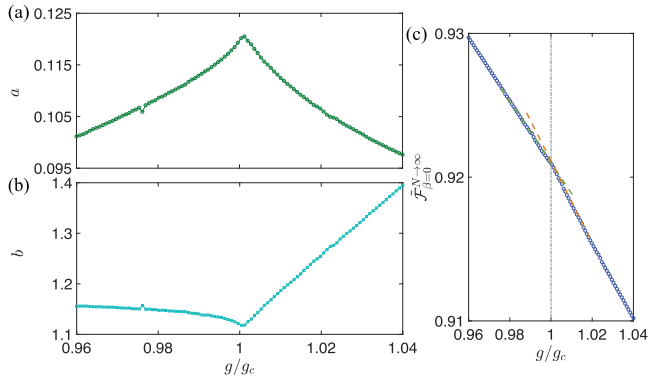

Figure 11. The coefficients a) a, b) b, and c) c in Equation (5) as functions of g/g_c.

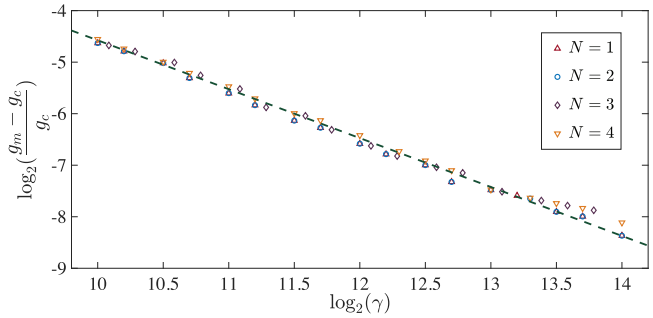

Figure 12. The dependence of $\log_2(\frac{g_m-g_c}{g_c})$ and $\log_2(\gamma)$ where g_m/g_c denotes the location of $\tilde{\mathcal{F}}_{\beta=0}$ minimum point in the Dicke model with $N = 1, 2, 3, 4$. The dashed lines are linear fittings with the formulation $\log_2(\frac{g_m-g_c}{g_c}) \approx -0.949\log_2(\gamma)$.

can pinpoint the critical point. Moreover, $\tilde{\mathcal{F}}^{N\to\infty}_{\beta=0} = 1 - c$ can be regarded as the value of $\tilde{\mathcal{F}}_{\beta=0}$ in the thermodynamic limit $N \to \infty$. The result of the coefficient c depicted in Figure 11c suggests that $\tilde{\mathcal{F}}_{\beta=0}$ can still characterize QPT in this limit.

It is now recognized that in the Dicke model, the quantity $\gamma = \Omega N/\omega_0$ dominates the criticality.[40] We proceed to explore the the finite-γ scaling law of $\tilde{\mathcal{F}}_{\beta=0}$, which can be regarded as the universal properties of all the finite-N Dicke model. As shown in **Figure 12**, the formulation of scaling law is

$$\log\left(\frac{g_m - g_c}{g_c}\right) \approx -\kappa \log(\gamma) \tag{6}$$

where g_m/g_c denotes the location of $\tilde{\mathcal{F}}_{\beta=0}$ minimum point. The scaling exponents κ and k play crucial roles in the universality of QPTs. Comparing the results in Figure 7b and Figure 12, it is revealed that $\kappa \simeq k$ and the QPTs in the Rabi and Dicke models belong to the same universality class. Consequently, the scaling laws of $\tilde{\mathcal{F}}_{\beta=0}$ are not only helpful for estimating the location of critical point with finite-η and finite-N, but also determining the universal class of QPTs. We also note that the formulation of scaling law Equation (6) is consistent with the results of the ground state energy in few-body Dicke model with finite-η shown in Figure 8c.

3. Conclusion and Outlook

We have presented numerical evidence showing that the time-averaged infinite-temperature OTOC $\tilde{\mathcal{F}}_{\beta=0}$ displays a minimum around the critical points in both the Rabi and Dicke models. In this way, the infinite-temperature OTOC dynamically diagnoses the QPT between normal phase and superradiant phase. In finite-frequency system, the QPT does not happen at the exact critical point calculated from the infinite-frequency system, which will give a finite-frequency scaling law. The scaling laws of $\tilde{\mathcal{F}}_{\beta=0}$ are identified to confirm the occurrence of QPTs. In the Rabi model, we show that the $\tilde{\mathcal{F}}_{\beta=0}$ present finite-frequency scaling behaviors close to the critical point. In the Dicke model, we also demonstrate the scaling behaviors of $\tilde{\mathcal{F}}_{\beta=0}$ with finite values of $\gamma = \Omega N/\omega_0$. The scaling laws are of great significance for phase transition. Based on the scaling laws, we characterize the QPTs in the limit $\gamma \to \infty$ from the data of OTOC with finite values of γ. Moreover, the universality class of QPTs has been identified by the scaling exponent obtained from the scaling laws. We find that the QPTs of the Dicke models with different number of atom(s) N belong to the same universality class, that is, the N-body Dicke models ($N = 1$ for the Rabi model), share a common scaling law.

This work may shed light on the characterization of QPT via the dynamics of Rényi entropy (RE) based on the OTOC-RE theorem.[27] Actually, the quenched dynamics of Rényi entropy has been widely studied in many-body systems theoretically[68] and experimentally.[69,70] Nevertheless, the quenched dynamics of Rényi entropy in cavity–atom interaction systems and its linkage between the QPTs and chaos in the systems are worthwhile to study further. On the other hand, this work could also enlighten the investigations of thermal-averaged OTOCs in condensed-matter systems[71–73] and other quantum optics systems such as driven Tavis–Cummings model.[67] With the rapid development of quantum simulation[46,48–54,74–76] and general measurement protocol of OTOCs,[77] we believe that our results may provide an experimentally feasible approach to detect equilibrium quantum critical points and find the universal properties of few-body systems in quantum region.

Supporting Information

Supporting Information is available from the Wiley Online Library or from the author.

Acknowledgements

Z.-H.S. and J.-Q.C. contributed equally to this work. J.-Q.C. thanks Ming Gong for helpful discussions. The authors are grateful to the numerical packages of the Python, Numpy, Scipy, and QuTiP open source projects. Y.H. was partially supported by National Natural Science Foundation of China (Grant No. 11774114). H.F. was partially supported by Ministry of Technology of China (Grant Nos. 2016YFA0302104 and 2016YFA0300600), National Natural Science Foundation of China (Grant No. 11774406), and Chinese Academy of Science (Grant No. XDPB0803).

Conflict of Interest

The authors declare no conflict of interest.

© 2020 WILEY-VCH Verlag GmbH & Co. KGaA, Weinheim

Keywords

Dicke model, out-of-time-order correlators, quantum phase transitions, Rabi model

Received: June 21, 2019
Revised: January 1, 2020
Published online:

[1] S. Sachdev, *Quantum Phase Transitions*, Cambridge University Press, Cambridge **2011**.
[2] X.-G. Wen, *Quantum Field Theory and Many Body Systems*, Oxford University Press, Oxford **2007**.
[3] H. bernien, S. Schwartz, A. Keesling, H. Levine, A. Omran, H. Pichler, S. Choi, A. S. Zibrov, M. Endres, M. Greiner, V. Vuletić, M. D. Lukin, *Nature* **2017**, *551*, 579.
[4] J. Zhang, G. Pagano, P. W. Hess, A. Kyprianidis, P. Becker, H. Kaplan, A. V. Gorshkov, Z.-X. Gong, C. Monroe, *Nature* **2017**, *551*, 601.
[5] U. Mishra, H. Cheraghi, S. Mahdavifar, R. Jafari, A. Akbari, *Phys. Rev. A* **2018**, *98*, 052338.
[6] B. Zŭnkovicˇ, M. Heyl, M. Knap, A. Silva, *Phys. Rev. Lett.* **2018**, *120*, 130601.
[7] M. Heyl, *Phys. Rev. Lett.* **2014**, *113*, 205701.
[8] S. H. Shenker, D. Stanford, *J. High Energy Phys.* **2014**, *03*, 067.
[9] S. H. Shenker, D. Stanford, *J. High Energy Phys.* **2015**, *05*, 132.
[10] P. Hosur, X.-L. Qi, D. A. Roberts, B. Yoshida, *J. High Energy Phys.* **2016**, *02*, 004.
[11] W. Buijsman, V. Gritsev, R. Sprik, *Phys. Rev. Lett.* **2017**, *118*, 080601.
[12] A. M. García-García, B. Loureiro, A. Romero-Bermúdez, M. Tezuka, *Phys. Rev. Lett.* **2018**, *120*, 241603.
[13] I. García-Mata, M. Saraceno, R. A. Jalabert, A. J. Roncaglia, D. A. Wisniacki, *Phys. Rev. Lett.* **2018**, *121*, 210601.
[14] J. Chávez-Carlos, B. López-del-Carpio, M. A. Bastarrachea-Magnani, P. Stránský, S. Lerma-Hernández, L. F. Santos, J. G. Hirsch, *Phys. Rev. Lett.* **2019**, *122*, 024101.
[15] N. Y. Yao, F. Grusdt, B. Swingle, M. D. Lukin, D. M. Stamper-Kurn, J. E. Moore, E. A. Demler, *arXiv*:1607.01801, **2016**.
[16] B. Swingle, G. Bentsen, M. Schleier-Smith, P. Hayden, *Phys. Rev. A* **2016**, *94*, 040302(R).
[17] A. Bohrdt, C. B. Mendl, M. Endres, M. Knap, *New J. Phys.* **2017**, *19*, 063001.
[18] M. McGinley, A. Nunnenkamp, J. Knolle, *Phys. Rev. Lett.* **2019**, *122*, 020603.
[19] C.-J. Lin, O. I. Motrunich, *Phys. Rev. B* **2018**, *97*, 144304.
[20] J. Bao, C.-Y. Zhang, *arXiv*: 1901.09327, **2019**.
[21] R. J. Lewis-Swan, A. Safavi-Naini, J. J. Bollinger, A. M. Rey, *Nat. Commun.* **2019**, *10*, 1581.
[22] R. Prakash, A. Lakshminarayan, *arXiv*: 1904.06482, **2019**.
[23] R.-Q. He, Z.-Y. Lu, *Phys. Rev. B* **2017**, *95*, 054201.
[24] X. Chen, T. Zhou, D. A. Huse, E. Fradkin, *Ann. Phys.* **2017**, *529*, 1600332.
[25] Y. Huang, Y.-L. Zhang, X. Chen, *Ann. Phys.* **2017**, *529*, 1600318.
[26] C. B. Dağ, L.-M. Duan, *Phys. Rev. A* **2019**, *99*, 052322.
[27] R. Fan, P. Zhang, H. Shen, H. Zhai, *Sci. Bull.* **2017**, *62*, 707.
[28] E. J. Torres-Herrera, A. M. García-García, L. F. Santos, *Phys. Rev. B* **2018**, *97*, 060303(R).
[29] H. Shen, P. Zhang, R. Fan, H. Zhai, *Phys. Rev. B* **2017**, *96*, 054503.
[30] Y. Alavirad, A. Lavasani, *Phys. Rev. A* **2019**, *99*, 043602.
[31] M. Heyl, F. Pollmann, B. Dóra, *Phys. Rev. Lett.* **2018**, *121*, 016801.
[32] M. Gärttner, J. G. Bohnet, A. Safavi-Naini, M. L. Wall, J. J. Bollinger, A. M. Rey, *Nat. Phys.* **2017**, *13*, 781.
[33] J. Li, R. Fan, H. Wang, B. Ye, B. Zeng, H. Zhai, X. Peng, J. Du, *Phys. Rev. X* **2017**, *7*, 031011.
[34] L. Bakemeier, A. Alvermann, H. Fehske, *Phys. Rev. A* **2012**, *85*, 043821.
[35] N. Lambert, C. Emary, T. Brandes, *Phys. Rev. Lett.* **2004**, *92*, 073602.
[36] C. Emary, T. Brandes, *Phys. Rev. Lett.* **2003**, *90*, 044101.
[37] C. Emary, T. Brandes, *Phys. Rev. E* **2003**, *67*, 066203.
[38] X.-Y. Lü, L.-L. Zhang, G.-L. Zhu, Y. Wu, *Phys. Rev. Appl.* **2018**, *9*, 064006.
[39] M.-J. Hwang, R. Puebla, M. B. Plenio, *Phys. Rev. Lett.* **2015**, *115*, 180404.
[40] M. Liu, S. Chesi, Z.-J. Ying, X. Chen, H.-G. Luo, H.-Q. Lin, *Phys. Rev. Lett.* **2017**, *119*, 220601.
[41] Y. Wang, W.-L. You, M. Liu, Y.-L. Dong, H.-G. Luo, G. Romero, J. Q. You, *New J. Phys.* **2018**, *20*, 053061.
[42] B.-B. Wei, X.-C. Lv, *Phys. Rev. A* **2018**, *97*, 013845.
[43] L.-T. Shen, Z.-B. Yang, H.-Z. Wu, S.-B. Zheng, *Phys. Rev. A* **2017**, *95*, 013819.
[44] J. Vidal, S. Dusuel, *Europhys. Lett.* **2006**, *74*, 817.
[45] J. Vidal, S. Dusuel, T. Barthel, *J. Stat. Mech.: Theory Exp.* **2007**, *2007*, P01015.
[46] K. Baumann, C. Guerlin, F. Brennecke, T. Esslinger, *Nature* **2010**, *464*, 1301.
[47] K. Baumann, R. Mottl, F. Brennecke, T. Esslinger, *Phys. Rev. Lett.* **2011**, *107*, 140402.
[48] J. Klinder, H. Keßler, M. Wolke, L. Mathey, A. Hemmerich, *Proc. Natl. Acad. Sci. USA* **2015**, *112*, 3290.
[49] M. P. Baden, K. J. Arnold, A. L. Grimsmo, S. Parkins, M. D. Barrett, *Phys. Rev. Lett.* **2014**, *113*, 020408.
[50] D. Lv, S. An, Z. Liu, J.-N. Zhang, J. S. Pedernales, L. Lamata, E. Solano, K. Kim, *Phys. Rev. X* **2018**, *8*, 021027.
[51] R. Puebla, M.-J. Hwang, J. Casanova, M. B. Plenio, *Phys. Rev. Lett.* **2017**, *118*, 073001.
[52] F. Yoshihara, T. Fuse, S. Ashhab, K. Kakuyanagi, S. Saito, K. Semba, *Nat. Phys.* **2017**, *13*, 44.
[53] Q.-T. Xie, S. Cui, J.-P. Cao, L. Amico, H. Fan, *Phys. Rev. X* **2014**, *4*, 021046.
[54] A. Crespi, S. Longhi, R. Osellame, *Phys. Rev. Lett.* **2012**, *108*, 163601.
[55] J. R. Johansson, P. D. Nation, F. Nori., *Comput. Phys. Commun.* **2012**, *183*, 1760.
[56] Online Supporting Information including the python codes and a documentation for the codes.
[57] T. J. Osborne, *Rep. Prog. Phys.* **2012**, *75*, 022001.
[58] I. M. Georgescu, S. Ashhab, F. Nori, *Rev. Mod. Phys.* **2014**, *86*, 153.
[59] D. Braak, *Phys. Rev. Lett.* **2011**, *107*, 100401.
[60] H. Gharibyan, M. Hanada, B. Swingle, M. Tezuka, *arXiv*: 1902.11086, **2019**.
[61] P. Hauke, M. Heyl, L. Tagliacozzo, P. Zoller, *Nat. Phys.* **2016**, *12*, 778.
[62] V. N. Popov, S. A. Fedotov, *Sov. Phys. JETP* **1988**, *67*, 535.
[63] D. S. Shapiro, A. N. Rubtsov, S. V. Remizov, W. V. Pogosov, Y. E. Lozovik, *Phys. Rev. A* **2019**, *99*, 063821.
[64] Y.-J. He, J. Zhou, S.-P. Li, Z.-H. Sun, *Quantum Inf. Process.* **2018**, *17*, 320.
[65] N. Shammah, S. Ahmed, N. Lambert, S. D. Liberato, F. Nori, *Phys. Rev. A* **2018**, *98*, 063815.
[66] A. Mezzacapo, U. L. Heras, J. S. Pedernales, L. DiCarlo, E. Solano, L. Lamata, *Sci. Rep.* **2014**, *4*, 7482.
[67] M. Feng, Y. P. Zhong, T. Liu, L. L. Yan, W. L. Yang, J. Twamley, H. Wang, *Nat. Commun.* **2015**, *6*, 7111.
[68] Y. O. Nakagawa, M. Watanabe, H. Fujita, S. Sugiura, *Nat. Commun.* **2018**, *9*, 1635.
[69] R. Islam, R. Ma, P. M. Preiss, M. E. Tai, A. Lukin, M. Rispoli, M. Greiner, *Nature* **2015**, *528*, 77.
[70] A. M. Kaufman, M. E. Tai, A. Lukin, M. Rispoli, R. Schittko, P. M. Preiss, M. Greiner, *Science* **2016**, *353*, 794.

 © 2020 WILEY-VCH Verlag GmbH & Co. KGaA, Weinheim

[71] C. B. Dağ, K. Sun, L.-M. Duan, *Phys. Rev. Lett.* **2019**, *123*, 140602.
[72] C. B. Dağ, L.-M. Duan, K. Sun, *arXiv*: 1906.05241, **2019**.
[73] B.-B. Wei, G. Sun, M.-J. Hwang, *Phys. Rev. B* **2019**, *100*, 195107.
[74] K. Xu, J.-J. Chen, Y. Zeng, Y.-R. Zhang, C. Song, W. Liu, Q. Guo, P. Zhang, D. Xu, H. Deng, K. Huang, H. Wang, X. Zhu, D. Zheng, H. Fan, *Phys. Rev. Lett.* **2018**, *120*, 050507.
[75] C. Neill, P. Roushan, M. Fang, Y. Chen, M. Kolodrubetz, Z. Chen, A. Megrant, R. Barends, B. Campbell, B. Chiaro, A. Dunsworth, E. Jeffrey, J. Kelly, J. Mutus, P. J. J. O'Malley, C. Quintana, D. Sank, A. Vainsencher, J. Wenner, T. C. White, A. Polkovnikov, J. M. Martinis, *Nat. Phys.* **2016**, *12*, 1037.
[76] Q. A. Turchette, C. J. Myatt, B. E. King, C. A. Sackett, D. Kielpinski, W. M. Itano, C. Monroe, D. J. Wineland, *Phys. Rev. A* **2000**, *62*, 053807.
[77] B. Vermersch, A. Elben, L. M. Sieberer, N. Y. Yao, P. Zoller, *Phys. Rev. X* **2019**, *9*, 021061.

© 2020 WILEY-VCH Verlag GmbH & Co. KGaA, Weinheim